Eur. Phys. J. A **11**, 297–304 (2001)

THE EUROPEAN PHYSICAL JOURNAL A

I. The properties of hot Ca-like fragments from the ^{40}Ca + ^{40}Ca reaction at 35 AMeV

R. Płaneta[1,a], W. Gawlikowicz[1], A. Wieloch[1], J. Brzychczyk[1], T. Ciszek[1], A.J. Cole[2], P. Désesquelles[2], K. Grotowski[1,4], P. Hachaj[1], S. Micek[1], P. Pawłowski[1], Z. Sosin[1], D. Benchekroun[3], E. Bisquer[3], A. Chabane[2], M. Charvet[2], B. Cheynis[3], A. Demeyer[3], E. Gerlic[3], A. Giorni[2], D. Guinet[3], D. Heuer[2], P. Lautesse[3], L. Lebreton[3], A. Lléres[2], M. Stern[3], L. Vagneron[3], and J.B. Viano[2]

[1] M. Smoluchowski Institute of Physics, Jagellonian University, Reymonta 4, 30-059 Cracow, Poland
[2] Institut des Sciences Nucléaires de Grenoble, IN2P3-CNRS/ Université Joseph Fourier 53, Avenue des Martyrs, F-38046 Grenoble Cedex, France
[3] Institut de Physique Nucléaire de Lyon, IN2P3-CNRS/ Université Claude Bernard 43, Boulevard du 11 Novembre 1918, F-69622 Villeurbanne Cedex, France
[4] H. Niewodniczański Institute of Nuclear Physics, Radzikowskiego 152, 31-342 Cracow, Poland

Received: 12 March 2001 / Revised version: 18 May 2001
Communicated by D. Guerreau

Abstract. The creation of hot Ca-like fragments was investigated in the ^{40}Ca +^{40}Ca reaction at 35 AMeV. Using the AMPHORA 4π detector system, the primary projectile-like fragment was reconstructed and its properties were determined. Both primary and secondary distributions are compared with the predictions of a Monte Carlo code describing a heavy-ion collision as a two-step process. Some of the nucleons which are identified as participants in the first step are transferred in the second step to these final states, which correspond on the average to the maximum value of entropy (thermodynamic probability). The model allows for competition between mean-field effects and nucleon-nucleon interactions in the overlap zone of the interacting nuclei. The analysis presented here suggests a thermalized source picture of the decay of the projectile-like fragment. The validity of the reconstruction procedure for projectile-like fragments is discussed.

PACS. 25.70.Gh Compound nucleus – 25.70.Lm Strongly damped collisions – 25.70.Pq Multifragment emission and correlations

1 Introduction

Many experiments in recent years have been devoted to investigating heavy-ion collisions in the intermediate energy region, between 10 and 100 AMeV. It has been shown that the emission of light particles (LP), which predominates below 10 AMeV [1], is gradually supplemented at higher energies by the production of intermediate mass fragments, IMFs, with atomic numbers $Z > 2$ [2]. The relatively simple reaction picture at low energies —with complete fusion, deep inelastic collisions (DICs) and quasi-elastic collisions appearing consecutively as the value of the impact parameter increases— becomes considerably more complicated above 10 AMeV. Various sources of LPs and IMFs have been observed and identified with hot projectile-like fragments (PLFs), target-like fragments (TLFs), evaporation residues, mid-rapidity sources and pre-equilibrium sources. The relative strengths of these various sources change with increasing energy. The PLF and TLF sources dominate at lower energies. At high energies they become spectators, while the overlap zone becomes most active. For central collisions, the complete fusion mechanism is transformed into incomplete fusion, and at highest energies into "full stopping", where most of the particles are probably emitted from the mid-rapidity source [3].

Interesting changes in the reaction mechanism are expected to occur around the Fermi energy. For lower energies, a di-nuclear system is briefly formed, and the effective flow of nucleons between the projectile and the target nucleus is governed mainly by the mean field, although fluctuations should also be included [4]. Energy damping in the system before break-up into a PLF and a TLF is mainly the product of one-body dissipation [5]. At higher energies, where the Fermi energy is negligible compared to the average nucleon kinetic energy, the Pauli principle is less effective in restricting two-body dissipation.

In the vicinity of the Fermi energy, the situation is more complex. Here, individual nucleon-nucleon (NN) col-

[a] e-mail: ufplanet@cyf-kr.edu.pl

lisions and residual Pauli blocking are thought to be important, as are mean-field effects. The experimental evidence in this energy region is not conclusive. Although it is generally accepted that the reaction has a predominantly binary character, an intermediate velocity source has been seen here in some experiments [6]. The degree of equilibration of the particle sources observed in the reaction is also unclear.

Due to the high multiplicity and diversity of the particles emitted, experimental investigation of heavy-ion reactions in this energy region also poses a considerable challenge, requiring sophisticated multi-detector systems and special filters to select various particle sources.

The aim of the present paper is to describe a study of the mechanism of ^{40}Ca+^{40}Ca collisions near the Fermi energy, at 35 AMeV. In this paper we will concentrate on the binary aspects of this reaction and on the properties of the hot Ca-like fragments. The formation of the intermediate velocity source is described in our second paper in this issue [6]. Using a 4π detector system it is possible not only to study the secondary decay products (as in many previous works) but also, using a reconstruction procedure, to obtain information on the primary reaction stage, where two hot Ca-like nuclei are formed.

Experimental data will be compared with the predictions produced by a model which allows for competition between mean-field effects and NN interactions in the overlap zone of the interacting nuclei. The model assumes a two-stage reaction scenario. In the first stage, a certain number of nucleons become reaction participants due to mean-field effects or the effects of NN interactions. In the second reaction stage, these nucleons either escape into continuum or are transferred to definite final states, creating a PLF, a TLF, or a cluster. The excited system decays afterwards due to particle emission. A detailed description of the model is presented in the third paper [7].

The fact that we can obtain information concerning both the hot nucleus and its decay products provides a unique opportunity to confront the model predictions with our data for both the creation and the decay of the hot PLF produced in the primary deep inelastic collision.

The primary events have been reconstructed for similar reactions by Lléres *et al.* [8,9] and by Péter *et al.* [3]. In [8,9], the hot PLF was reconstructed for Ca + Cu collisions at 35 AMeV. Using the azimuthal angular distributions of alpha-particles, the correlation between the PLF excitation energy and the angular momentum has been extracted and compared to the predictions of the classical trajectory model [10], and to the Cole random walk model [11]. The de-excitation of the PLF has been compared to the predictions of the GEMINI [12] and percolation models for different bins of the excitation energy of the primary PLF [13]. Péter *et al.* [3] studied the Ar + Al reaction at energies from 55 to 95 AMeV. The reconstructed mass and excitation energy of the PLF were used as input for model calculations, and afterwards compared to the secondary data. Other aspects of the ^{40}Ca + ^{40}Ca reaction, studied at 35 AMeV in another experiment, have been investigated by Hagel *et al.* [14, 15]. The reaction mechanism has been investigated for a similar, nearly symmetric Ar + KCl system in the energy range 32–74 AMeV [16]. It has been demonstrated that the collisions are mostly binary.

A brief description of our experiment, together with important features of the data, is presented in sect. 2. A more detailed description of the experimental procedure can be found in [17–19]. These papers are devoted to the special filters used to select different particle sources, including more central collisions. The reconstruction of the sources is described in sect. 3, and the decay properties of the hot Ca-like nuclei are discussed in sect. 4. The Monte Carlo code used in this work is briefly presented in sect. 5, and its predictions are compared to the experimental data in sect. 6. The efficiency of the filters and of the PLF reconstruction procedure is discussed in sect. 7. The final section contains a summary and the conclusions.

2 The experimental procedure

The experiment was performed with a 1.4 GeV Ca beam from the Grenoble SARA facility. The beam was focused on a 0.5 mg/cm^2 Ca target located inside an AMPHORA detector system [20], which covers about 80% of 4π. In our experiment, 30 gas ionization chambers were placed in front of the CsI detectors, instead of thin scintillator foils, lowering the energy thresholds to about 1 AMeV. This installation was made for two detector rings at 31.2 and 46.6 degrees LAB [21].

The elastic scattering of ^{4}He, ^{12}C, ^{16}O, and ^{20}Ne ions at four different energies was used to calibrate the IMF energy.

The total kinetic energy of the fragments, which is important for the reconstruction of the PLFs, may be influenced by random coincidences [19]. To avoid this effect, no on-line multiplicity triggers were applied, and low beam intensity was used. In addition windows were set on time spectra in order to clean out data from accidental coincidences coming from different beam bursts.

As we know from model simulations [17,18] for our reaction with the AMPHORA detector's software filter [22], damped binary collisions represent the major part of the observed cross-section for this relatively light system, even for events where at least 75% of the total entrance channel charge was detected.

In order to study the properties of the ^{40}Ca +^{40} Ca reaction's binary channels over a wide range of dissipation energy, we retained all events with a total collected charge greater than 5. For such events, the mean value of the total charged-particle multiplicity is 9.4, whereas the value obtained for more complete events is 12 [17]. The mean value of the total collected charge, $\langle Z_{\rm tot}\rangle$, is 22.3, which indicates that, on the average, we detect about one-half of the system's total charge. In the case of quasi-elastic collisions and DIC, we detect mostly the PLF moving with a near beam velocity, together with light particles. The kinetic energy of the TLF is mostly below the system's detection thresholds.

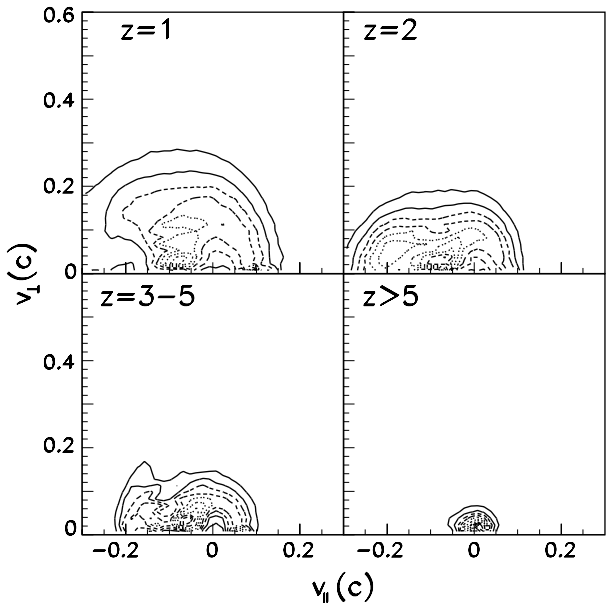

Fig. 1. Galilean invariant-velocity plots (linear scale) in the rest frame of the reconstructed PLF with the parallel velocity axis oriented by the PLF CM velocity, for different groups of particles ($p_{\rm tr} < 4.5$ GeV/c).

It was demonstrated by Péter *et al.* [3], and will be shown for our system in sects. 3 and 7, that the selection of events with a sufficiently high-measured value, $p_{\rm par}$, of the total parallel momentum enables a reasonable reconstruction of the PLF. Hereafter, we will refer to such events ($p_{\rm par} > 8$ GeV/c) as "well defined", and only these events will be used for further analysis.

3 Source identification and reconstruction of the PLF

Since in our events we collect on the average no less than one-half of the entrance channel charge we can, in principle, determine the PLF velocity, charge, mass and excitation energy.

The PLF reconstruction procedure is usually performed in two steps (see *e.g.* [3]). In the first step one must construct, for each event, the velocity vector of the center of mass of the primary PLF from the momentum vectors of the products. The second step involves estimating the charge, mass, and excitation energy of the primary PLF. For a successful reconstruction, possible contamination from sources other than PLF should, of course, be minimized.

We approximate the primary PLF velocity vector by using the CM velocity of fragments with $Z \geq Z_{\rm min} = 3$. We also require their velocities to be larger than the reaction's CM velocity. Particles with smaller Z values are excluded from this procedure, since they may be coming from other sources.

Figure 1 presents the Galilean invariant velocity distributions of different groups of particles ($Z = 1$, $Z = 2$, $Z = 3$–5 and $Z > 5$) in the reference frame of the primary PLF. The X-axis of this reference frame is oriented along the PLF velocity vector in the CM of the total system. These distributions are shown for events with the total transverse momentum, $p_{\rm tr} < 4.5$ GeV/c , which is used here as a measure of the dissipated energy. Emission from one source, the hot PLF nucleus, is observed for heavier ejectiles. Some contribution from other sources is seen at negative velocities. This admixture is more pronounced for light particles.

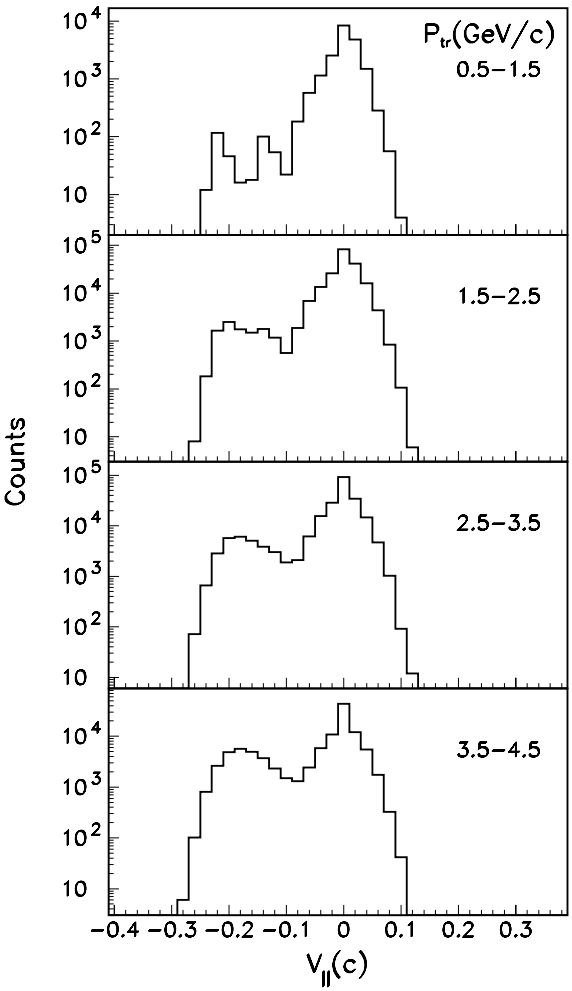

Fig. 2. Projection of the distribution of fig. 2 on the $v_{\|}$ axis for consecutive windows of $p_{\rm tr}$.

For the class of heaviest fragments, $Z > 5$, we present a projection of the distributions of fig. 1 on the $v_{\|}$ axis (fig. 2). This plot was made for consecutive windows in the transverse momentum. For all values of $p_{\rm tr}$, we observe a strong maximum located at the center of mass of the reconstructed PLF ($v_{\|} = 0$). An additional, weaker maximum at negative values of $v_{\|}$ originates mostly from the TLF. This is not observed in fig. 1, due to the linear vertical scale. Its contribution increases along with the increasing value of $p_{\rm tr}$.

In the next step of the reconstruction procedure, the primary PLF charge is calculated, event by event. The

charges of all those IMFs for which the parallel velocity component in the rest frame of the primary PLF is larger than $-0.1c$ are totaled. IMFs with lower velocity values are assumed to come from other sources (see figs. 1 and 2). For $Z < Z_{\min}$ we take only particles emitted in the forward hemisphere, and multiply their number by two. In this way we minimize the contribution of light particles coming from other sources.

In order to estimate the primary PLF mass, a mass equal to $2Z$ is assumed for each IMF. For those particles for which $Z < Z_{\min}$, the masses of all the fragments emitted in the forward hemisphere are summed up and multiplied by two. It is also assumed that in each event the number of emitted neutrons is equal to the number of emitted protons. This is expected to be a reasonable approximation for the ^{40}Ca $+^{40}$ Ca symmetric system.

The calorimetric method is used to estimate the excitation energy. The kinetic energies of the fragments in the rest frame of the PLF are summed up with the same restrictions as for the reconstruction of charge and mass. The contribution of light particles ($Z < Z_{\min}$) emitted in the forward hemisphere is multiplied by two. The summed kinetic energy of the neutrons is assumed to be equal to that of the protons, minus the Coulomb energy. Finally, we include the involved Q value, estimated using particle masses.

The distribution of the reconstructed PLF mass ($A_{\rm PLF}$) is presented in fig. 3a for consecutive $p_{\rm tr}$ windows. The average value of this distribution is located for the first two windows slightly below the projectile mass, which may imply the existence of an intermediate velocity source. A slight shift towards larger $A_{\rm PLF}$ values and a large mass tail observed for increasing $p_{\rm tr}$ values may be due to some admixture of the TLF and other sources (note the position of the $v_{\rm PLF} > -0.1c$ cut in fig. 2). The width of the $A_{\rm PLF}$ distribution increases with the $p_{\rm tr}$, and is considerably larger for the highest $p_{\rm tr}$ value.

The reconstructed PLF excitation energy distributions are shown in fig. 3b for the same $p_{\rm tr}$ windows. The average excitation energy and the width of its distribution increase for larger $p_{\rm tr}$. For those bins with higher $p_{\rm tr}$ the excitation energy distributions cover practically the full range of energy available in the CM system.

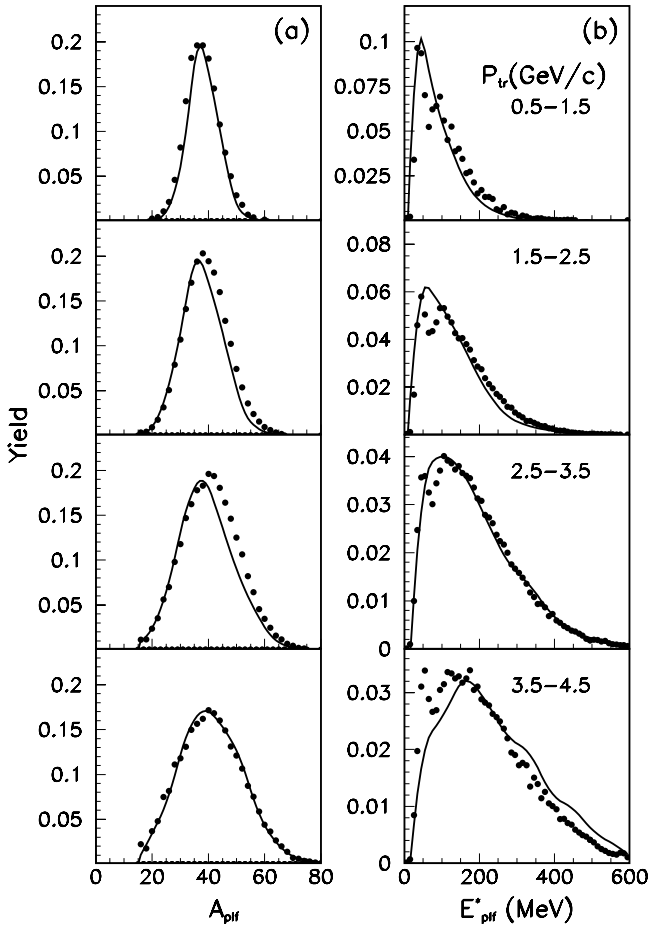

Fig. 3. Mass (a), and excitation energy (b) distributions of the reconstructed PLF for consecutive $p_{\rm tr}$ windows. Experimental points and model predictions.

4 The decay properties of the hot PLF fragment

Figure 4 presents the charge distributions of the decay products for consecutive bins in the PLF excitation energy, E^*/A. The group of light particles is about 10 times stronger than the IMFs, which form some kind of plateau up to about $Z = 15$ for lower E^*/A, and up to $Z = 11$ for higher E^*/A values.

It should be mentioned that in heavier systems, such as Xe + Sn, studied with INDRA [23], one finds that heavier IMFs are preferentially emitted from the neck region. In the lighter system ^{40}Ca + ^{40}Ca, there is probably not enough matter in the neck. In fact, we have isolated an intermediate velocity source of mainly lighter particles, located in the reaction center of mass. As shown in sect. 7, its contribution is eliminated in the reconstruction procedure for more peripheral collisions. The observation and description of the intermediate velocity source is the subject of our second paper in this issue [6].

Figure 5 presents the angular distribution of the decay fragments in the frame of the reconstructed PLF, for heavier fragments ($Z > 5$) which are less contaminated by other sources. If the memory of the initial direction of the projectile is lost, the angular distribution should exhibit forward-backward symmetry, which can indeed be observed in fig. 5, with reasonable accuracy. This fact may be taken as an argument in favor of "loss of memory". The concave shape of the distribution suggests a relatively high spin value of the decaying PLF. The model presented in the next section predicts here $22\hbar$ (average value). The angular distribution of fig. 5 was made for events with at least two $Z > Z_{\min}$ fragments used in the PLF reconstruction procedure. A similar distribution shape is obtained for events with three such fragments.

Figure 6 shows the energy distributions of protons and alphas. They are presented in four windows of PLF excitation energy. Systematic variation in the distribution slope

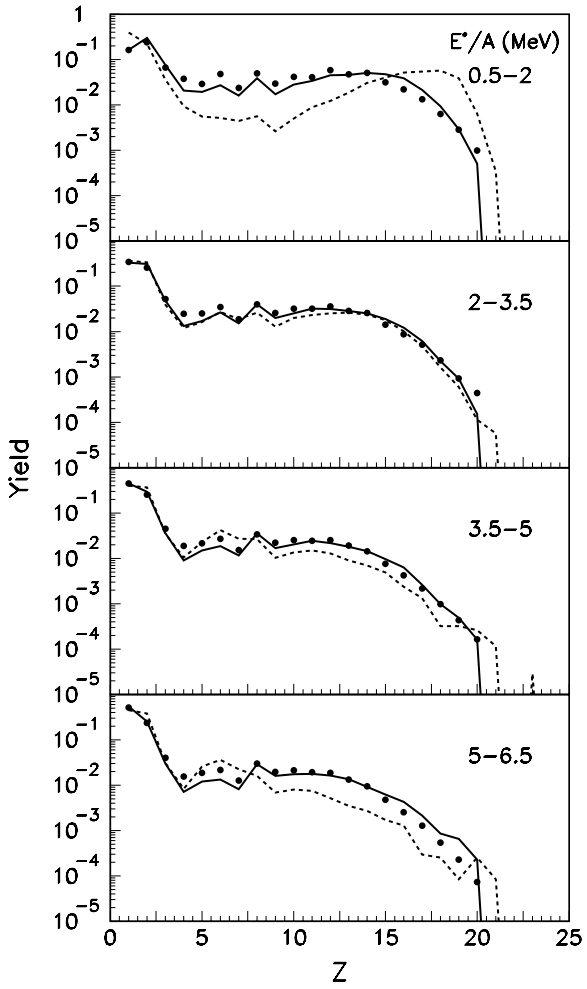

Fig. 4. Charge distributions of particles from the PLF source, for consecutive bins of the PLF excitation energy. Experimental points and model predictions: with the experimental filter (solid lines) and without the experimental filter (dashed lines). The model distributions have been normalized to the same surface.

parameter with excitation energy is observed for both ejectiles.

5 The model (Monte Carlo code)

In order to describe the mechanism of the ^{40}Ca + ^{40}Ca reaction in the vicinity of the Fermi energy, we used a computer Monte Carlo code called PIRAT, based on a model proposed by Sosin [7].

The model assumes a two-stage reaction scenario:

In the first stage, a certain number of nucleons becomes reaction participants as a result of mean-field effects or two-nucleon interaction. In the mean-field mechanism, a nucleon belonging to the projectile (P) or to the target (T) nucleus becomes a participant when it runs across a potential window opening between colliding heavy ions. The degree of opening depends on the proximity and relative velocity of the heavy ions on their classical Coulomb

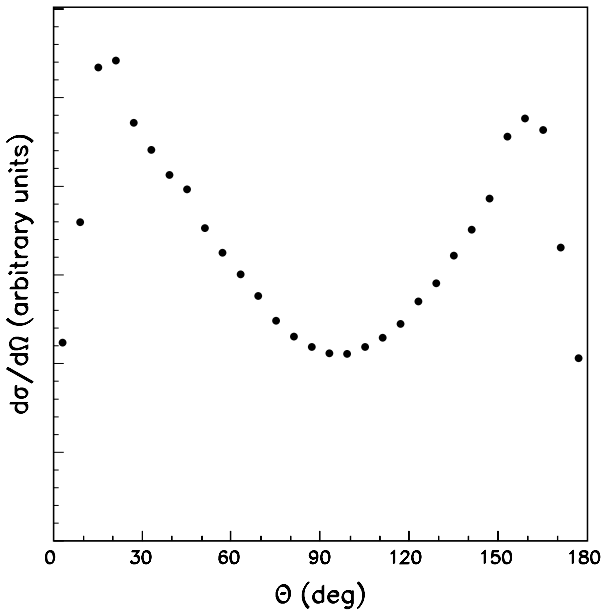

Fig. 5. Angular distributions of $Z > 5$ decay fragments in the reference frame of the reconstructed PLF.

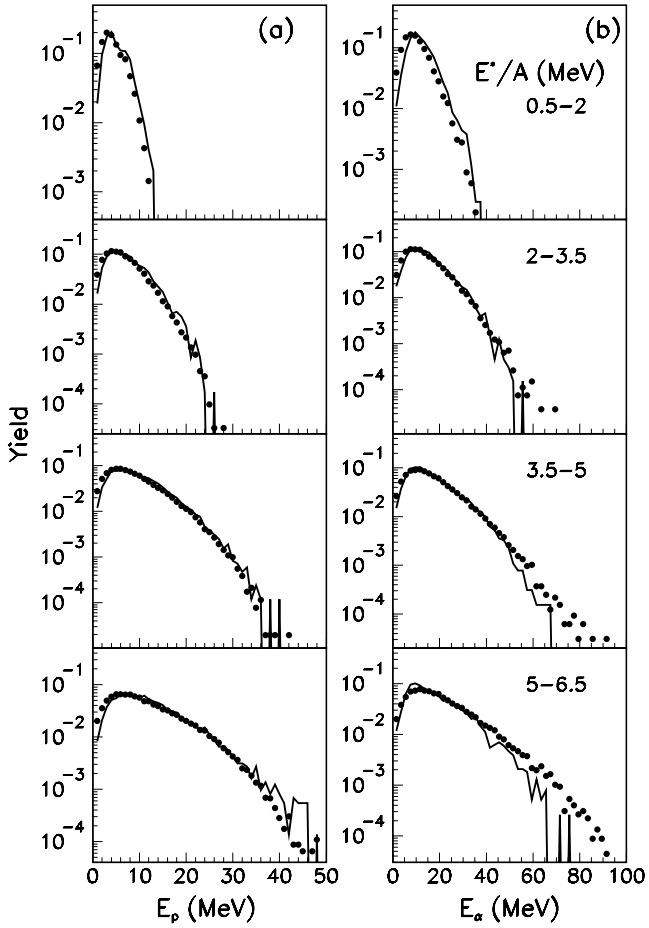

Fig. 6. Energy spectra for protons (a), and alpha particles (b), emitted from the PLF for different bins of the PLF excitation energy. Experimental points and model predictions.

trajectories. In the two-nucleon mechanism, two nucleons, one from the P and the other from the T nucleus, undergo a nucleon-nucleon interaction in the overlap zone of the P and T nuclei, where the Pauli principle becomes less restrictive. The probability of such an interaction depends on the NN interaction cross-section, the available momentum space and on the convolution of the P and T densities in the overlap region.

The relative contribution of the mean-field mechanism and the two-nucleon mechanism depends on the heavy-ion collision energy. For our reaction at 35 AMeV, this amounted to an average of 25% and 75%, respectively. It also depends on the collision impact parameter. The mean-field contribution increases for more central collisions. For details, see our third paper in this issue [7].

The nucleons which are identified as participants in the first reaction stage are transferred in the second stage to these final states, which correspond on the average to the maximum value of the density of states of the system (a statistical assumption). Fluctuations characteristic of the stochastic process are taken into account. In this way, the PLF, the TLF or a set of clusters is created. Some of the participating nucleons may escape into the continuum.

The angular momenta and spins of the final reaction products are calculated from the initial P and T, and from the angular momenta of the participating nucleons involved. Their values are necessary in order to define limiting transfer conditions for the participating nuclei (see [7]) and as input to the GEMINI [12] subroutine which simulates the decay of the excited fragments.

The charged fragments produced according to the reaction scenario described above have individual velocities and are accelerated in the mutual Coulomb field along trajectories, which are integrated numerically [24]. The predictions made by the model are filtered by a software replica of the AMPHORA detector system [22].

6 Model predictions and comparison with experimental data

The PLF mass and excitation energy distributions predicted by the model are displayed in figs. 7a and 7b for consecutive windows in angular momentum.

For peripheral collisions, the primary PLF mass distribution is narrow and centered at a mass just below 40 (fig. 7a). There is a slight shift indicating the emission of prompt particles. The distribution becomes much broader and shifted for more central collisions, where the number of participants is larger and the contribution from the intermediate velocity source is more important (see our third [7] and second paper in this issue [6]).

As would be expected, the primary average PLF excitation energy increases and its distribution broadens for more central collisions (fig. 7b).

The angular momentum L (impact parameter) is not experimentally measurable; instead, we have used here the total transversal momentum of the charged particles detected. The $p_{\rm tr}$ *vs.* L dependence is monotonic but considerably diffused (see fig. 8). As a result, a $p_{\rm tr}$ window

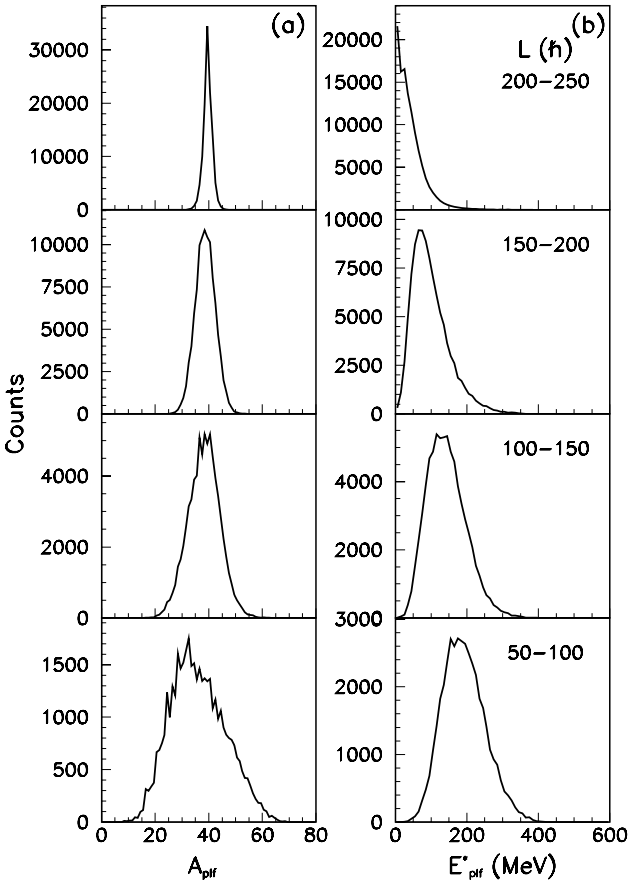

Fig. 7. Primary PLF mass (a), and excitation energy (b) distributions predicted by the model for consecutive bins of angular momentum L.

contains quite a broad range of different L values. Nevertheless, $p_{\rm tr}$ can be used as a rough measure of the total dissipated energy. As seen in figs. 3a and 3b, the model properly predicts the shapes of the reconstructed experimental PLF mass and excitation energy distributions for consecutive bins in $p_{\rm tr}$. The slight broadening observed in figs. 3a and 3b is induced by the reconstruction procedure. In particular the high-energy tails of the excitation energy distributions predicted by the model are much shorter (fig. 7b) than the reconstructed ones (fig. 3b).

The agreement is generally also good on the secondary reaction level. The particle Z distributions (fig. 4), as well as the energy distributions of the protons and alphas emitted by the PLF (fig. 6), are quite well reproduced in the consecutive bins of the PLF reconstructed excitation energy. In fig. 4 the unfiltered, model predicted charge distributions are also presented in order to judge the bias introduced by the AMPHORA detector.

7 The validity of the PLF reconstruction procedure

The aim of the PLF reconstruction procedure described in sect. 3 is to extract, event by event, the particles orig-

Table 1. Average percentage participation of the primary PLF source in the total reconstructed PLF mass and excitation energy, predicted by the model.

$Z_{\min} = 6$		
$p_{\rm tr}$ window (GeV/c)	$A_{\rm PLF}$(rec)	$(E^*/A)_{\rm PLF}$(rec)
0.5–1.5	99	96
1.5–2.5	98	92
2.5–3.5	95	84
3.5–4.5	88	74
$Z_{\min} = 3$		
$p_{\rm tr}$ window (GeV/c)	$A_{\rm PLF}$(rec)	$(E^*/A)_{\rm PLF}$(rec)
0.5–1.5	99	94
1.5–2.5	98	90
2.5–3.5	94	83
3.5–4.5	86	72

inating from the PLF decay, and to minimize the influence of other sources. As presented in figs. 3, 4 and 6, the predictions made by the PIRAT code are generally in agreement with the experimental data. One may well ask, however, if this means that, when using our reconstruction procedure, we are indeed seeing the properties of the PLF source, or rather the properties of a system containing, beside the PLF, also contributions from other sources. This question can be answered by tagging the particles in the model which originate from PLF decay and those from the decay of other sources. It was found that the efficiency of the PLF reconstruction procedure depends slightly on the minimum charge, $Z_{\min}$, defined in sect. 3. Table 1 presents the average percentage participation of the PLF source in the reconstructed PLF mass $A_{\rm PLF}$(rec), and the excitation energy $(E^*/A)_{\rm PLF}$(rec) predicted by the model for different $p_{\rm tr}$ windows. The calculations were made for $Z_{\min} = 3$, and for $Z_{\min} = 6$. As shown by table 1, the reconstructed PLF source for $Z_{\min} = 6$ and 0.5 GeV/c < $p_{\rm tr}$ < 1.5 GeV/c contains 99% of the primary PLF mass and 96% of the primary PLF excitation energy. These numbers drop to 95% and 84%, respectively, in the 2.5–3.5 GeV/c window. For $Z_{\min} = 3$, contamination by other sources is slightly worse. Clearly we may reasonably speak of a reconstructed PLF source only for an upper limit of $p_{\rm tr}$, which depends upon the problem under discussion.

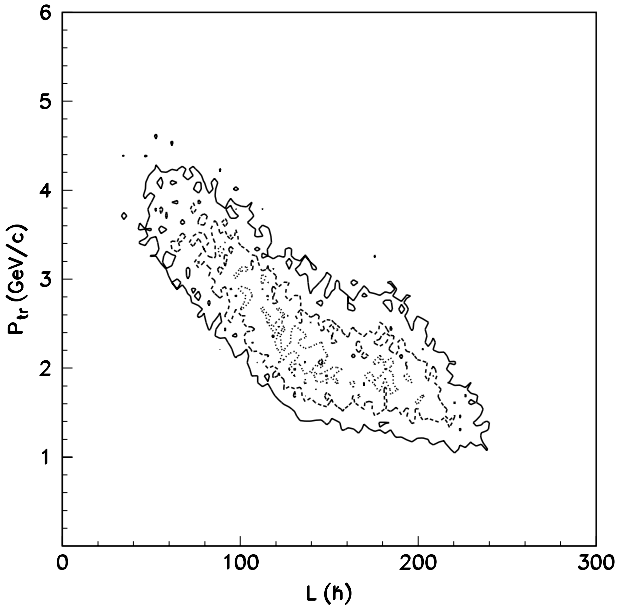

Fig. 8. The dependence $p_{\rm tr}$ *vs.* L; model prediction.

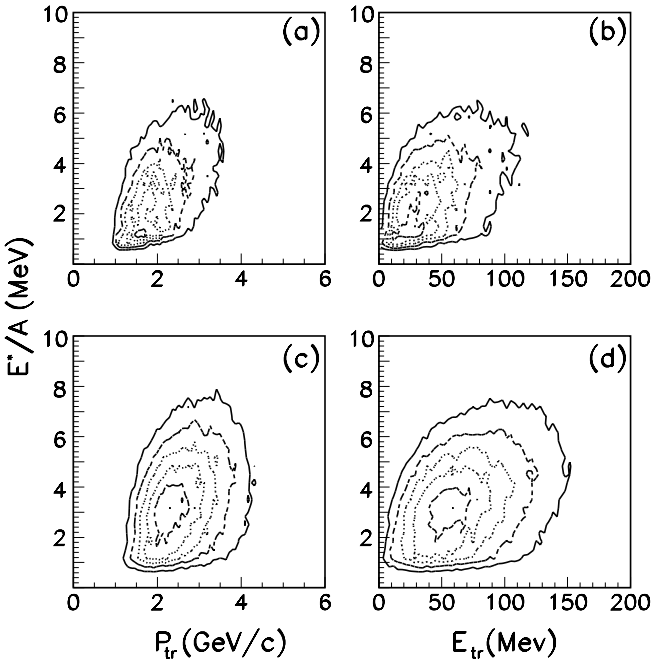

Fig. 9. Two-dimensional plots: (a) E^*/A *vs.* $p_{\rm tr}$, and (b) E^*/A *vs.* $E_{\rm tr}$ (experimental data); (c) E^*/A *vs.* $p_{\rm tr}$, and (d) E^*/A *vs.* $E_{\rm tr}$ (model predictions).

Another problem related to the reconstruction procedure is the degree of auto-correlation, which may affect the data presented. Figure 9 displays E^*/A *vs.* $p_{\rm tr}$ and E^*/A *vs.* $E_{\rm tr}$ for the experimental data (a), (b), and for the model predictions (c), (d). Here $E_{\rm tr}$ is the transversal energy obtained for light-charged particles only. As can be seen, the two dependencies appear to be similar for experimental data and for model predictions. We have also determined that the distributions presented in figs. 4 and 6 appear to be similar in all $E_{\rm tr}$ windows.

8 Summary and conclusions

The ^{40}Ca + ^{40}Ca reaction at 35 AMeV was used to study the mechanism of heavy-ion collisions in the Fermi energy domain. The 4π detection system enabled us to reconstruct the primary projectile-like fragments for both quasi-elastic and more inelastic collisions. The charge, mass and excitation energy distributions of the primary PLFs were determined. The de-excitation of the PLF source was also studied.

The width of the reconstructed primary PLF mass distribution increases with increasing $p_{\rm tr}$, while its average value remains close to the projectile mass. The primary PLF excitation energy increases with increasing $p_{\rm tr}$, and its width also increases.

The shape of the energy spectra of particles from the PLF decay is consistent with a thermalized source picture. The forward-backward symmetry of the angular distribution observed in the frame of the reconstructed PLF also suggests some sort of "loss of memory". The model predicts here the PLF average spin value $22\hbar$.

The experimental data are fairly well described by the two-stage reaction scenario which forms the basis of the PIRAT Monte Carlo computer code [7]. Here a certain number of nucleons become participant in the first reaction stage as a result of mean-field effects or NN interactions in the overlap zone of the colliding nuclei. In the second reaction stage, these nucleons are transferred to final states, which on the average correspond to the maximum value of entropy (thermodynamic probability). The thermodynamic probabilities are governed by the distribution of the density of states of the various subsystems taking part in the heavy-ion collision, allowing the fluctuations characteristic of a stochastic process.

By using this model one may describe the creation and decay of three different hot sources of particles produced in a heavy-ion collision, the PLF, the TLF and the IVS (see [6]). As far as we know, it was not previously possible.

It is also possible to separate the contributions made by different sources to the reconstructed PLF mass and excitation energy. The quality of separation depends on a sufficiently large $Z_{\rm min}$ value for the particles used to determine the reconstructed PLF velocity vector. The possibility to reconstruct a hot source properly selected from other sources is quite important to study, for example, its thermal properties [25].

The decay of the excited fragments is simulated in the PIRAT code using the GEMINI [12] or alternatively the SIMON [26] subroutine. It was found that the agreement between model predictions and experimental data is better for the GEMINI subroutine, which uses the Hauser-Feshbach formalism to describe the evaporation of light particles.

This work was supported by the Scientific Research Commission of Poland (KBN Grant PB 1188/P03/98/14) and the M. Skłodowska-Curie Fund (MEN/DOE- 97-318). Calculations for this work were partly performed using facilities of the Cracow Academic Computing Center, CYFRONET (KBN Grant No. S2000/UJ/023/1998).

References

1. See for example, W.U. Schröder, J.R. Huizenga, in *Treatise on Heavy-Ion Science*, edited by D.A. Bromley, Vol. **2** (Plenum Press, New York and London) 1984, pp.113-726.
2. See B. Borderie et al. Phys. Lett. B **205**, 26 (1988); W.U. Schröder, Nucl. Phys. A **538**, 439c (1992); Z. Sosin et al., Nucl. Phys. A **574**, 474 (1994).
3. J.Péter et al., Nucl. Phys. A **593**, 95 (1995).
4. W.J. Świątecki, Phys. Scripta **24**, 113 (1981); O. Mazonka, C. Jarzyński, J. Błocki, Nucl. Phys. A **641**, 335 (1998).
5. J. Błocki et al., Ann. Phys. (N.Y.) **113**, 330 (1978).
6. Z. Sosin et al., this issue, p. 305.
7. Z. Sosin, this issue, p. 311.
8. A. Lléres et al., Phys. Rev. C **48**, 2753 (1993).
9. A. Lléres et al., Phys. Rev. C **50**, 1973 (1994).
10. J.R. Birkelund, L.E. Tubbs, J.R. Huizenga, J.N. De, D. Sperber, Phys. Rep. **56**, 107 (1979).
11. A.J. Cole,R. Cherkaoui-Tadili, J. Alarja, Phys. Rev. C **40**, 1265 (1989).
12. R.J. Charity et al., Nucl. Phys. A **483**, 371 (1988).
13. P. Désesquelles et al., Phys. Rev. C **48**, 1828 (1993).
14. K. Hagel et al., Phys. Rev. Lett. **68**, 2141 (1992).
15. K. Hagel et al., Phys. Rev. C **50**, 2017 (1994).
16. V. Métivier et al., Nucl. Phys. A **672**, 357 (2000).
17. P. Pawłowski et al., Z. Phys. A **357**, 387 (1997).
18. P. Pawłowski et al., Phys. Rev. C **54**, R10 (1996).
19. P. Pawłowski et al., Phys. Rev. C **57**, 1771 (1998).
20. D. Drain et al., Nucl. Instrum. Methods A **281**, 528 (1989).
21. T. Barczyk et al., Nucl. Instrum. Methods A **364**, 311 (1995).
22. M.E. Brandan et al., Nucl. Instrum. Methods A **334**, 461 (1993).
23. E. Plagnol et al., Phys. Rev. C **61**, 014606 (2000).
24. W. Gawlikowicz, Acta Phys. Pol. B **28**, 7 (1997).
25. M. D'Agostino et al., Nucl. Phys. A **650**, 320 (1999).
26. D. Durand, unpublished.